Journal of Arid Environments 182 (2020) 104260

Contents lists available at ScienceDirect

Journal of Arid Environments

journal homepage: www.elsevier.com/locate/jaridenv

On the performance of microlysimeters to measure non-rainfall water input in a hyper-arid environment with focus on fog contribution

Christian Feigenwinter *, Joel Franceschi, Jarl Are Larsen, Robert Spirig, Roland Vogt

Department of Environmental Sciences, Atmospheric Sciences, University of Basel, Switzerland

ARTICLE INFO

Keywords:
NRWI (Non-rainfall water input)
Microlysimeter
Fog deposition
Fog precipitation
Hyper-arid environments
NaFoLiCA
Central Namib Desert

ABSTRACT

The measurement of non-rainfall atmospheric water input (NRWI) in arid environments requires instruments that are capable to detect even smallest amounts of total daily water input of less than 0.1 mm. Microlysimeters yield robust and high precision data of such low NRWI. We provide a technical description of a self-constructed microlysimeter and demonstrate its excellent performance regarding the analysis of NRWI in the Central Namib Desert. Three stations of the FogNet measurement network have been equipped with microlysimeters in order to measure fog deposition. NRWI and evaporation for days/nights without fog shows a persistent diurnal course. Deviations from this baseline define the amount of fog deposition, intensity and duration of a fog events. A more detailed analysis of a five-day period reveals the complex nature and variation between individual fog events with respect to the different patterns of fog deposition and fog precipitation and the contribution of adsorption, dew and fog to NRWI. The relation between fog precipitation and fog deposition is not straightforward and a simple parameterization of the processes that quantifies the amount of the water sampled by fog collectors and its connection to NRWI is still lacking.

1. Introduction

Fog deposition, i.e. the direct input of water into an ecosystem by fog, is one of three components of non-rainfall water input (NRWI) beside dew and water vapour adsorption water (WVA). Because NRWI is an important source of water for plants and animals in hyper-arid environments, a better understanding and quantification of NRWI components is essential (e.g. Seely et al., 1998; Wang et al., 2017; Zheng et al., 2018; Kidron and Starinsky, 2019; Mitchell et al., 2020). Albeit the significance of this process for water-limited ecosystem functions is well established, no standard procedure for measuring NRWI exists and NRWI itself, and its vectors, is subject to different interpretations in the scientific literature. In theory, the components of NRWI are well defined (e.g. Agam and Berliner, 2006): i) fog occurs, independent of surface conditions, when the atmospheric water vapour concentration is close to 100%, i.e. reaches saturation. The deposition of fog droplets onto a surface is a function of settling rate and the interception with objects; ii) dew forms usually during the night on objects near the ground if the land surface temperature (*LST*) is lower than or equal to the dew point temperature but still above 0 °C; iii) Water from the atmosphere is adsorbed in the pores of the uppermost soil layer when air relative humidity is higher than the relative humidity in the soil pores and *LST* is higher than the dew point temperature, tendentially in the late afternoon. A comprehensive review on dew formation and adsorption processes in semi-arid regions is given in Agam and Berliner (2006) and Kidron and Starinsky (2019).

In practice, it is challenging to partition the total NRWI into its components because the processes are often superimposed, e.g. fog and dew or dew and WVA, though the formation mechanisms are different. The partitioning of NRWI vectors (Uclés et al., 2014) is additionally complicated by the fact that evaporation and deposition may occur simultaneously and thus reduce total NRWI during fog events (Wrezinsky et al., 2004; Beiderwieden et al., 2008), e.g. when cloud-penetrating solar radiation heats the surface and the near-surface air and leads to evaporation of the fog droplets. A possible method to distinguish dew from fog and its origin is the analysis of stable isotopes (Kaseke et al., 2017). The quantification of deposition rates of less than 0.01 mm (Agam and Berliner, 2006) and the partitioning of NRWI requires instruments that are able to resolve even smallest amounts of water input changes.

Several devices can measure NRWI and its components, but, contrary to rainfall, no standard method exists. In the following a short summary

* Corresponding author.
E-mail address: christian.feigenwinter@unibas.ch (C. Feigenwinter).

https://doi.org/10.1016/j.jaridenv.2020.104260
Received 24 March 2020; Received in revised form 8 July 2020; Accepted 9 July 2020

of most common measurement methods with a special focus on microlysimeters is given:

- Microlysimeters (MLs) are an effective method for measuring NRWI, as they are able to measure all three vectors with a sufficient accuracy (Uclés et al., 2014). Several studies (Graf et al., 2004; Heusinkveld et al., 2006; Kaseke et al., 2012; Uclés et al., 2013) presented automated MLs that continuously record the weight of a sampling container allowing determination of the amount and the duration of NRWI and evapotranspiration (ET). Most available studies use such self-constructions of various designs (e.g. Ninari and Berliner, 2002; Agam and Berliner, 2004a; Heusinkveld et al., 2006; Kaseke et al., 2012; Uclés et al., 2013). Only recently a commercial version of a ML has been placed on the market (Smart Field Lysimeter, METER Group, Inc. USA). All designs basically follow the principle of placing an undisturbed soil sample in a container and then record its weight continuously or in predefined intervals. Though there is no official definition of the term ML, we consider devices with a total container weight below 20 kg and a matching load cell capacity as "microlysimeters". The dimension of the sampling container is dependent on the load cell characteristics and vice versa, i.e. a higher rated load cell allows for a larger sample size. The fact that a high resolution is required to resolve the very small deposition and evaporation rates of NRWI in hyper-arid regions makes MLs the ideal device for studies in bare soil or surfaces with sparse vegetation. If operated in arid and hyper-arid environments, where rainfall is rare and soils are generally dry, ML sampling containers are usually not equipped with a drainage. Therefore, the soil sample has to be replaced after the rare, but potentially heavy precipitation events and the device has to be recalibrated. Care must also be taken that the soil sample reflects the properties and the heat balance of the surrounding soil as close as possible. This concerns mainly the dimensions of the sample (surface area and depth) and the material of the container. The diameter of the MLs usually ranges from 0.07 up to 0.30 m but, to our knowledge, there are no studies that demonstrate an effect of change in the surface area on the representability of ML measurements. The depth of the ML soil sample is more crucial as it has to preserve the heat balance of the surrounding soil, i.e. the temperature and moisture profile, which theoretically requires a depth where the diurnal soil temperature is constant (Ninari and Berliner, 2002). In practice, Jacobs et al. (1999) demonstrated, that depths from 0.035 m to 0.075 m are considered sufficient for NRWI sampling in arid environments (the Negev Desert) as the daily moisture exchange processes occur in the uppermost layers of the soil, but the discussion about the ideal depth of the soil sample is still ongoing (Agam, 2014). Table 1 in Uclés et al. (2013) presents an overview on ML sampling container sizes in bibliography. Most MLs use a PVC protection to prevent the sampling container from damage and direct contact with the surrounding substrate. The load cell unit is normally mounted in a stable housing of various materials below the soil dish. To keep the load cell temperature as stable as possible it should be placed deep enough and the parts connecting the load cell with the sampling dish should be made with a material of low thermal conductivity.

A careful and proper installation in the field is crucial for the quality and accuracy of ML measurements. The surface of the soil sample must be level with the surrounding surface and the sample container must be mounted centred on the load cell to avoid imbalances. Soil movement, water entering the device during heavy rainfall and animal trampling are other possible sources of malfunction, often limiting ML measurements to a few weeks on maximum. Frequent calibration and visits at ML sites are mandatory for long-term time series of acceptable quality. Uclés et al. (2013) presented an installation and placement strategy for long-term ML measurements in a semi-arid steppe environment resulting in MLs data for consecutive 49 days.

Table 1
Geographical location of microlysimeter sites and main meteorological characteristics during the investigation periods IOP1 (Sep/Oct 2017) and IOP2 (Feb/Mar 2018).

		Coastal Met CM	Vogelfederberg VF	Gobabeb GB
Latitude/Longitude (°)		−23.056/14.626	−23.098/15.029	−23.561/15.041
Elevation (m a.s.l.)		94	515	406
Distance to coast (km)		17	56	58
Mean, max., min. daily temperature (°C)	IOP1	14.2 20.7 10.2	16.0 26.1 9.0	17.1 28.1 9.2
	IOP2	18.2 24.8 14.1	20.7 29.4 14.2	21.4 30.7 13.6
Mean daily max. shortwave downwelling radiation SW↓ (Wm^{-2})	IOP1	981	1026	1013
	IOP2	1018	1063	1048
#fog-days/#total days	IOP1	37/50	31/50	23/50
	IOP2	29/47	14/47	11/47

- Active and passive fog collectors comb out water from the atmosphere by a mesh or harp normally placed about 2 m a.g.l. Timing and quantity of collected fog water are generally recorded by a rain gauge and the water may be sampled for subsequent chemical, biological or isotopic analysis. Different designs and materials are used for the collectors, affecting fog water sampling efficiency and drainage, which has impacts on the interpretation of the sampled quantities within the hydrological cycle. The standard unit of amount of water per unit area (mm or l m^{-2}) is normally obtained by dividing the amount of sampled water by the projected area of the collector. Note that in this study fog precipitation is preferably given in ml, because the topic of how the vertically oriented area of a fog collector compares to the horizontal area of common precipitation and fog deposition measurements by MLs in detail is still not clarified. Common instruments are the standard fog collector (Schemenhauer and Cerceda, 1994), the Juvik-type fog gauge (Juvik and Nullet, 1995), the Grunow-type fog sampler (Grunow, 1952), harp-type collectors (Goodman, 1985) and active devices of Daube-type (Demoz et al., 1996). Several studies compare the performance of different fog samplers (e.g. Regalado and Ritter, 2017; Frumau et al., 2011; Fernandez et al., 2018) and theoretical work about the aerodynamics of collection efficiency and performance has been published (Rivera, 2011; Regalado and Ritter, 2016).
- Optical devices such as disdrometers, cloud droplet probes (CDP) and fog monitors (FM) (Eugster et al., 2006; Spiegel et al., 2012), as well as Particle Volume Monitors (PVM) (Gerber, 1991) are used to analyse the droplet size distribution and allow the calculation of liquid water content LWC, partially also in combination with Eddy Covariance systems.
- Eddy Covariance (EC) systems (e.g. Aubinet et al., 2012) measure the vertical turbulent exchange of water vapour, i.e. the latent heat flux, unless combined with an optical device. Note that fog water deposition derived from EC (e.g. Klemm et al., 2005) refers to deposition on the ground or on the surface below the EC system, i.e. in the vertical direction. Therefore, it may also be worth to take into account the non-turbulent vertical advection term (Lee, 1998) when calculating total deposition from a single EC tower. Horizontal advection may also play a major role for comparison with fog samplers. However, estimation of horizontal fluxes requires several EC towers (Feigenwinter et al., 2008) and thus, no studies have yet considered the influence of the non-turbulent advection terms on fog deposition. Additional drawbacks of the EC method in arid environments are the extremely small fluxes due to limited water availability and the reduced functionality if droplets are deposited on the sonic transducers. Furthermore, common EC systems usually do only

catch the gaseous phase of fog and do not account for the liquid phase, i.e. fog droplets, if not combined with an instrument to account for liquid water flux. Having said this, only few studies exist using the EC method for measuring NRWI. Klemm et al. (2005) measured fog deposition in a subalpine fir forest and Florentin and Agam (2017) concluded that NRWI (dew and WVA) estimations derived from EC latent heat flux during 7 clear days/nights tended to underestimate the flux compared to microlysimeter recordings.

- Dewmeters (e.g. Beysens et al., 2005) are usually horizontal metal plates allowing dew formation on the surface by radiative cooling, which is monitored by a load cell. Price and Clarke (2014) present a portable device consisting of a load cell upon which exchangeable types of natural and artificial canopies can be placed. Other direct measurement methods use artificial surfaces, e.g. a wooden block with a special coating (Duvdevani, 1947), absorbent cloths (Kidron, 2000) or glass plates (Beysens et al., 2005). A common drawback of these methods is difference to the natural surface of the investigation area, normally resulting in over- or underestimation of dew amount.
- Further supporting devices for the characterization of fog events are visibility instruments, leaf wetness sensors and ceilometers.

The object of this paper is to investigate the performance of MLs to measure NRWI into the soil with focus on fog deposition, deposition duration and the subsequent evaporation. We present ML data from two Intensive Observation Periods (IOPs) at three sites conducted in the frame of the Namib Fog Life Cycle Analysis project (NaFoLiCA) (Spirig et al., 2019). The performance of MLs is characterized with respect to i) resolution and precision of the load cell and calibration drift, ii) temperature dependence of the load cell, iii) dimensions of the sample container, iv) capability to separate fog deposition from dew and WVA input and v) determination of fog deposition amount and duration. The ML NRWI and fog deposition duration is then compared with data from other instruments (Juvik passive fog sampler, leaf wetness sensors, visibility meters and radiation) for a five-day case study period experiencing fog events of different character.

2. Materials and methods

2.1. Study area and measurement period

The measurements were performed in the Central Namib Desert at three sites of the FogNet infrastructure (Spirig et al., 2019) (Table 1 and Fig. 1). The base of the research activities within the NaFoLiCA project (Spirig et al., 2019) was the Gobabeb Namib Research Institute (gobabeb.org), a place of highest reputation in desert research since 1962 (Henschel and Lancaster, 2013). Climatological characteristics of the research area are those of a typical coastal desert similarly to the Peruvian/Atacama Desert with hyper-arid conditions and annual rainfall of less than 50 mm. Main site properties with mean daily average, maximum and minimum temperatures, mean daily maximum global radiation and the number of days with fog are given in Table 1. The dominant soil type for all three sites is characterized as “alluvium, sand, gravel, calcrete plains” (Mendelsohn et al., 2002), in fact a bare soil of sandy loam texture with almost no organic matter and moderate gravel content.

The measurements cover two Intensive Operation Periods (IOP1 and IOP2), when the ML stations were regularly visited and the MLs were checked for proper operation. IOP1 and IOP2 refer to the periods from 9 Sep to 28 Oct 2017 and from 10 Feb to 27 Mar 2018, respectively. Fig. 2 shows the cumulative change in water content (see section 3.1) of MLs during IOP1 and IOP2. Our main analysis focuses on the first phase of IOP1 (11 Sep until 1st Oct) where the most and strongest fog events occurred and continuous high quality ML time series from all three sites were available.

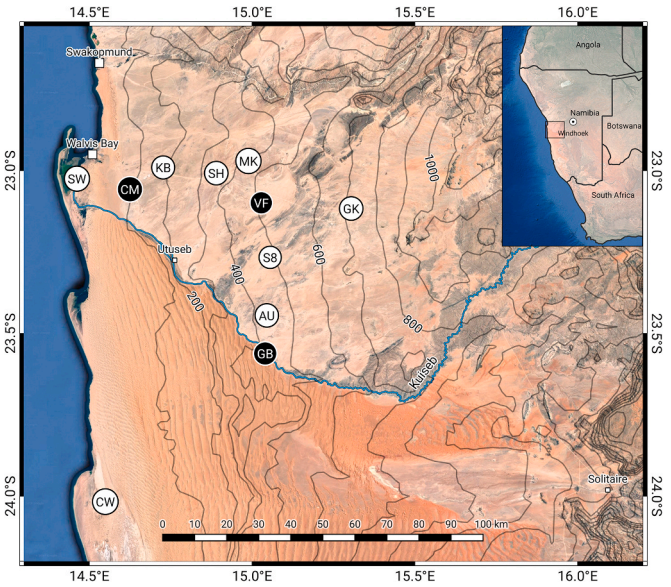

Fig. 1. Research area in the Central Namib and locations of the FogNet stations. Stations equipped with microlysimeters in black. Contour lines are derived from SRTM data, background imagery from Google Maps. Map inlay shows the research area in the larger context of south-western Africa.

2.2. Microlysimeter design and technical specification

2.2.1. Construction, dimensions and electronics

Our MLs follow the concept presented in Heusinkveld et al. (2006). The load cells with rated capacities of 7 kg and the electronics are housed in an aluminium cast box isolated on top with a 10 mm closed cell foam to reduce heat exchange with the soil above. The base of the box is at 0.3 m depth after installation. All other parts of the ML are made of polyvinylchloride (PVC) to minimize the heat exchange between the surface and the load cell assembly. The protective soil dish of the sampling container has holes at the bottom in order to let water drain into the surrounding soil in case of rain (occurred only once during IOP2). We used PVC soil dishes with a diameter of 0.25 m and a depth of 0.065 m (Fig. 3 and Fig. 5). We additionally constructed two smaller MLs with a diameter of 0.13 m, a depth of 0.035 m and a load cell with a rated capacity of 1 kg to assess the influences of surface area and depth of the soil probe. These two additional devices were installed at Gobabeb (GB) for comparison purposes.

The electronic circuit is shown in Fig. 4 and its components are listed in Table 2. The load cell is connected in a wheatstone bridge to a low-noise amplifier with a gain of 128 and a 24 bit delta-sigma analog-to-digital converter and is measured at 1 Hz. Data is stored temporarily in an Arduino Pro Mini, which also processes the signal from the temperature/humidity sensor inside the load cell housing. Each minute a Campbell CR1000 data logger collects the measured data over a serial connection (RS-232). All analogue signal processing takes place in the load cell housing to keep the temperature influence at a minimum.

2.2.2. Calibration

Initial tests in the lab showed that load cells need several days to stabilize after large load changes. This, in combination with the difficulties of bringing a calibrated scale capable of measuring the filled ML containers of 7 kg accurately and without disturbance into the field, led to the use of a relative calibration: The temporal change of the soil container mass relative to the mass at calibration time was used to derive NRWI. With this method, we got accurate information about the change in mass over time, without a priori knowledge of the total mass of the soil sample in the container. Three calibration weights with a respective mass of 2, 5 and 10 g were used (Fig. 5c). During calibration,

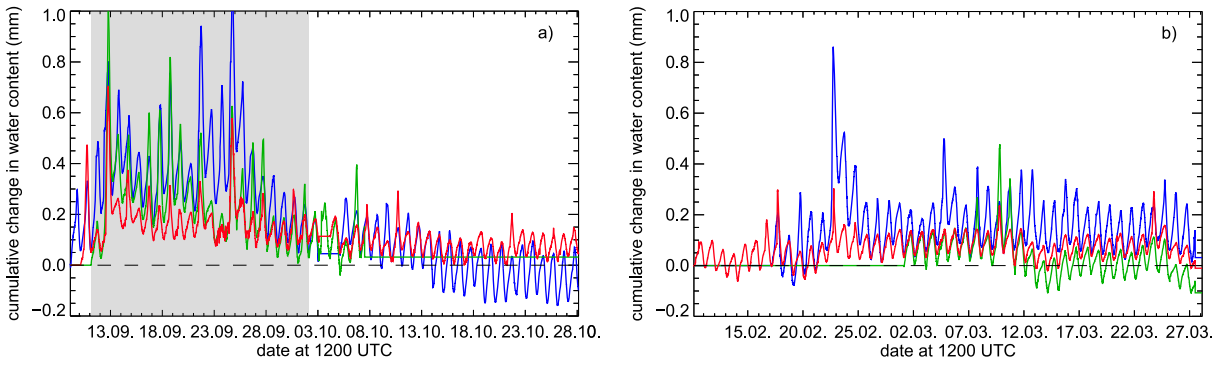

Fig. 2. Cumulative change in ML water content for IOP1 (a) and IOP2 (b) for CM (blue), VF (green) and GB (red). Shaded period refers to first phase of IOP1, which is analyzed in detail in this study. (For interpretation of the references to color in this figure legend, the reader is referred to the Web version of this article.)

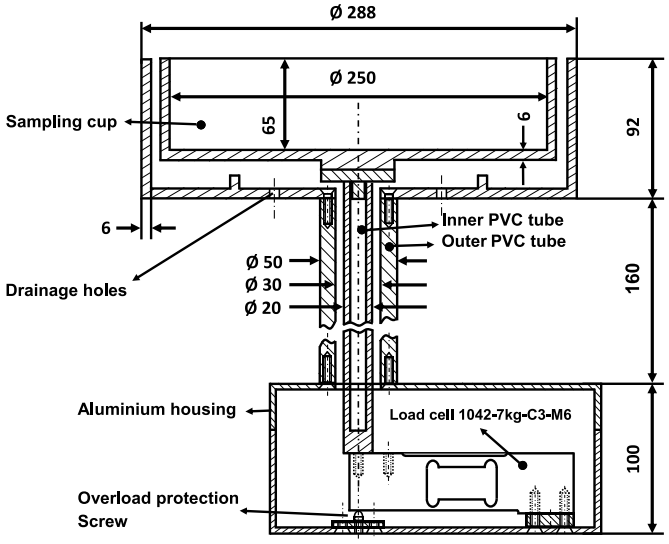

Fig. 3. Microlysimeter construction details. The soil sample dish is centred on a PVC rod fixed to the load cell. Electronics (Arduino, temperature and humidity sensor) are located adjacent to the load cell. Measures are given in mm.

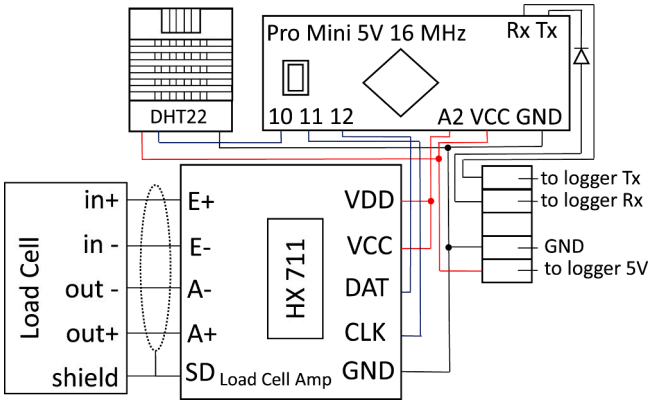

Fig. 4. *ML circuit board schematics.*

they were placed in the centre of the soil-filled MLs resulting in a sequence of total calibration mass of 0-2-7-17-15-10-0 g and thus 21 pairs of absolute true values. We let the scale stabilize for 1 min between each change of the calibration mass. The mean standard deviation during these stabilization periods was ±0.008 mm on average and defines the precision of the MLs. The calibration coefficient results from the slope of the linear regression. Accuracy was derived from the range

Table 2
Electronic circuit components and specifications.

Load cell	Tedea Huntleigh 1042-7 kg-C3-M6, total error 0,02% of rated output
Load cell amplifier/ADC	Sparkfun HX711 24 bit
Controller	Arduino Pro Mini 5V/16 MHz
Temperature/*RH* sensor	DHT 22, Accuracy: ± 0,5 °C ± 2% RH
Theoretical ML resolution	1.6 mg ≅ 3.2 × 10^{-5} mm water input (for 0.25 m diameter MLs)
ML field precision/ accuracy	±0.008 mm/0.005 mm
Data Logger	Campbell Scientific Ltd. CR1000

of deviations from the true value (i.e. the difference of absolute change in weight) for all possible pairs for each calibration event. The estimation of the total weight of the sampling container is derived by applying the calibration coefficient to the offset of the regression. The calibration coefficients and the gravitational properties of the soil samples of all MLs at all locations proved to be very stable during the investigation period (Table 3).

Considering the measured amounts of NRWI in the range of 0.1–0.2 mm the accuracy of 0.003 mm (median of all values in Table 3) is well suited to detect also small changes in a time interval of 10 min. This deposition rate was used to detect the duration of fog deposition during fog events (see section 3.1). In order to be sure that the observed increase of ML weight during nights without fog is not due to temperature effects in the load cell and the electronic circuit, ML2 at the GB site was covered with a waterproof lid for several nights (Fig. 6). The daily cycle of measured mass was almost completely removed and daily temperature variations in the load cell housing were in the range of 1–2 °C (Fig. 7b).

This implies that the observed daily variance of ML readings indeed reflects fluctuations due to changes in soil water content by exchange processes with the atmosphere. Nearby MLs are gradually drifting apart due to aeolian transport of sand resulting in an offset between the different devices. Apart from this offset, which is easily adjusted for by zeroing the record at the beginning of a new daily cycle (see section 3.1), MLs at the same location perform almost identically regardless of sampling size (Fig. 7a). Minor deviations are attributed to lee effects and shadow effects of the covering lid.

2.2.3. *ML housing temperatures and surface temperatures*

Temperatures in the load cell housings (MLT) agree well. Given the good agreement between MLTs, the small variation in weight of the covered ML2 is attributed to condensation/evaporation processes in the closed chamber forced by radiative heating/cooling of the lid (Fig. 7a). The daily amplitude in the range of 1 and 2 K for the large and the small MLs, respectively, is negligible if compared to the daily variation of air temperatures and surface temperatures in the range of about 20 K and

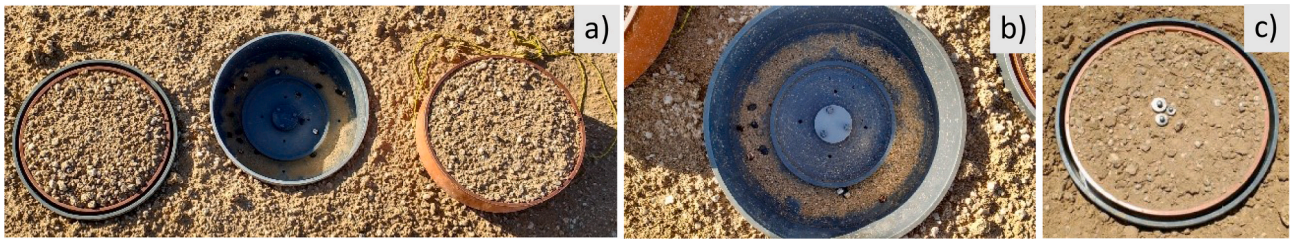

Fig. 5. MLs (0.25 m diameter) at Vogelfederberg. a) Sampling container of one ML removed. b) Sand and soil particles intruding between sampling container and protecting envelope are deposited on the bottom of the envelope, not affecting the measurements. Holes in the inner ring are for water drainage. c) ML with centrally placed weights during calibration on 7 Oct 2017

Table 3
Calibration results: slope of the regression from the calibration sequence (see text) in mg per raw load cell output. Total soil mass is derived by applying the calibration coefficient to the raw zero offset and sampling volume. Sampling container diameter is 0.25 m and ML depth is 0.065 m, unless otherwise stated. Accuracy and precision are calculated for each calibration event (see text). *diameter 0.13 m, depth 0.035 m.

ML site and #	Calibration date	Slope (mg/raw unit)	Estimated total sampling mass (kg)	Precision (mm) and (g)	Accuracy (mm)
CM ML1	12 Sep 2017	1.605921	4.641	0.003 (0.17)	0.003
	10 Oct 2017	1.618772	4.654	0.006 (0.28)	0.004
	14 Feb 2018	1.614739	4.474	0.002 (0.92)	0.001
CM ML2	12 Sep 2017	1.580542	4.439	0.006 (0.30)	0.003
	10 Oct 2017	1.561105	4.377	0.004 (0.20)	0.004
	14 Feb 2018	1.578644	4.262	0.004 (0.18)	0.003
VF ML1	27 Sep 2017	1.597921	5.941	0.003 (0.13)	0.001
	7 Oct 2017	1.644375	6.113	0.010 (0.51)	0.020
	16 Feb 2018	1.588324	5.872	0.004 (0.20)	0.004
VF ML2	27 Sep 2017	1.580865	5.837	0.005 (0.24)	0.001
	7 Oct 2017	1.580564	5.833	0.007 (0.33)	0.003
	16 Feb 2018	1.577620	5.779	0.002 (0.10)	0.002
GB ML1	13 Sep 2017	1.711519	6.965	0.017 (0.85)	0.013
GB ML2	13 Sep 2017	1.633894	7.092	0.023 (1.12)	0.006
	9 Feb 2018	1.610915	6.974	0.003 (0.15)	0.001
GB ML3*	13 Sep 2017	0.228421	0.911	0.021 (0.27)	0.017
	9 Feb 2018	0.227336	0.901	0.005 (0.06)	0.002
GB ML4*	13 Sep 2017	0.215259	0.976	0.019 (0.26)	0.008
All MLs average				0.008 (0.30)	0.005
All MLs median				0.005 (0.22)	0.003

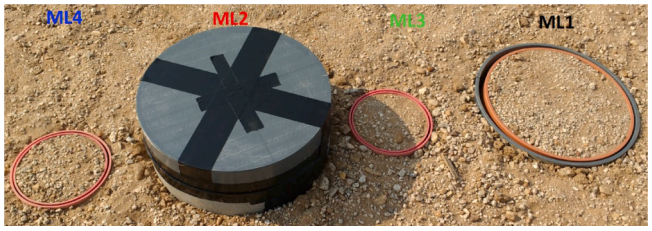

Fig. 6. The four MLs of different diameters (0.25 m and 0.13 m) at GB. ML2 is covered with a waterproof lid to test the performance and temperature dependence. ML text colors refer to line colors in Fig. 7. (For interpretation of the references to color in this figure legend, the reader is referred to the Web version of this article.)

35 K, respectively (Fig. 7b), and suggests that the box material and the depth of the base of the housing at −0.3 m are well suited to avoid large temperature amplitudes. The heating/cooling in the housings of the small MLs 3/4 occurs faster and results in a slightly larger amplitude (Fig. 7c). The two fog events (27/28 Sep and 30 Sep/1 Oct) during the ML test period give an estimate of the fog deposition amount relative to total NRWI. ML readings start to exceed the values of typical no-fog nights when visibility falls below 1000 m and the atmospheric water vapour concentration approaches saturation, i.e. air temperature is close to the dew point temperature. These periods coincide with elevated surface temperatures indicating a stratus/low cloud event (Fig. 7b). Note that dew point temperature T_{dew} is not directly measured but derived from relative humidity and air temperature by the August-Roche-Magnus approximation (Alduchov and Eskidge, 1996). Theoretically, dew only occurs when dew point temperature is equal or greater than the surface temperature. As shown in Fig. 7b, this occurs only for a short time in the early morning of 29 Sep and 1 Oct. Main NRWI contributions are therefore attributed to fog and water vapour adsorption at GB. A more comprehensive analysis of similar events is given in section 4.

Thermal images (VarioCAM® HD research 600, InfraTec GmbH, Dresden, Germany) of the ML surfaces in VF during the night from 27 Sep to 28 Sep 2017 together with *LST* (IR120, Campbell Scientific Ltd., at 1.9 m), and average soil temperatures (CS655, Campbell Scientific Ltd., at −0.1 m) document the representativity of the ML samples. The thermal images were corrected for an emissivity of 0.966 as reported for desert soil crust in Qin et al. (2005). The average surface temperatures of ML soil samples (circles with a radius of 50 pixels corresponding to about 13k pixels each) are compared to two reference plots (540 x 70 and 90 x 100 pixels) in the close surroundings, as defined in Fig. 8a) and shown in Fig. 8b).

In general, ML surface temperatures were slightly cooler than the surroundings due to isolation from deeper soil layer. The small gap between soil container and the protective cylinder shows the highest temperatures in the thermal image and represents a bulk temperature of the PVC surface areas seen by the camera in the volume between the ML sampling container and the protecting cylinder (see also Fig. 3). The location of the maximum values is dependent on the view angle of the IR-camera, i.e. the closer to nadir, the deeper the insight in the gap and

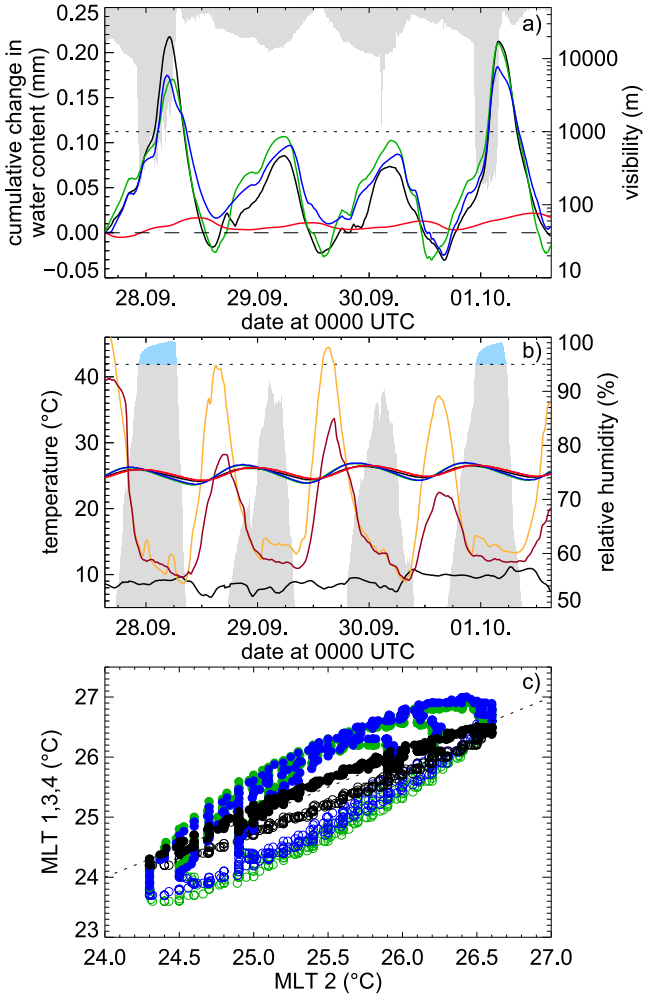

Fig. 7. ML1 (black), ML3 (green) and ML4 (blue) performance during 4 consecutive nights compared to covered ML2 (red). a) ML readings in mm. Visibility (grey areas, right axis) < 1000 m indicates fog events per WMO definition. Major ticks refer to midnight. b) same as a) but for load cell housing temperatures. Orange and black lines refer to air temperature, surface temperature and dew point temperature, respectively. Grey areas refer to relative humidity above 50% (right axis). RH > 95% (horizontal dotted line) indicates potential fog events. c) Housing temperatures MLT 1,3,4 versus MLT 2. Open symbols refer to 0300–1500 UTC. (For interpretation of the references to color in this figure legend, the reader is referred to the Web version of this article.)

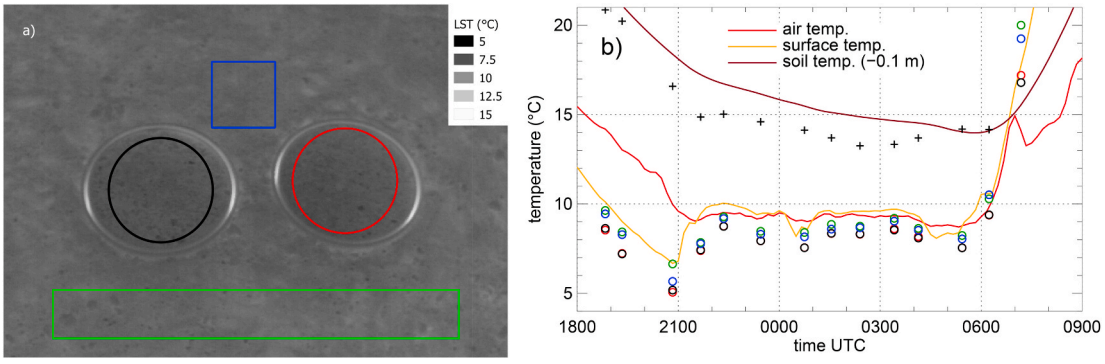

Fig. 8. a) Thermal image of VF MLs on 27 Sep at 2140 UTC with areas for ML1 (black), ML2 (red) and control plots of the surrounding soils (green, blue). b) Averaged surface temperatures of these areas (symbols), measured surface temperature (orange), air temperature (red), maximum image temperature (black crosses) and average soil temperature at −0.1 m (brown). (For interpretation of the references to color in this figure legend, the reader is referred to the Web version of this article.)

the higher the temperature. Maximum values are roughly in the range of the measured average soil temperatures in −0.1 m depth (Fig. 8b). During the night, when surface temperature and air temperature vary only slightly, differences between ML and control plots are lowest with the ML surfaces roughly 0.5 K colder than the surroundings. With the larger cooling/heating rates around sunset/sunrise the difference reaches up to 1 K and the standard deviations of ML surface temperatures are generally larger (not shown). We attribute this to a greater heterogeneity of the ML soil samples, because cooling/heating rates of MLs and reference subplots agree almost perfect, pointing to similar thermal inertia and demonstrating the representativeness of the MLs. These findings agree with Agam and Berliner (2004) and Uclés et al. (2013) for similar experiments. Nevertheless, the differences in surface temperatures should be kept in mind when interpreting the results. Note that we did not continue the experiment during daytime.

3. Duration of fog events and fog deposition

3.1. Duration of fog deposition

The deviation from the mean diurnal ML variation is used for the determination of fog deposition amount and duration. We define no-fog nights if no fog precipitation is recorded by the Juvik fog collectors or the maximum fog deposition is below a site-specific threshold, i.e. 0.07 mm, 0.11 mm and 0.13 mm for GB, VF and CM, respectively. The number of nights without fog at the ML stations can be derived from the last row in Table 1. IOP 1 was more affected by fog nights than IOP 2 and fog deposition was significantly reduced during IOP 2 reflecting the fog climatology of the research area (e.g. Andersen et al., 2019; Spirig et al., 2019).

All ML readings of no-fog days were averaged after setting each daily record (consisting of 144 records) to zero at the start of a new daily cycle at 1500 UTC to derive the baseline diurnal cycle of NRWI without fog deposition. Since the local time zone is UTC+2 this refers roughly to the time when NRWI usually starts, i.e. shortly before sunset. The mean diurnal course of MLs during nights without fog (Fig. 9) shows a persistent shape although standard deviations vary with site and season, but in general, the deviations are moderate. The mean maximum deposition amounts of 0.07 mm (GB), 0.11 mm (VF) and 0.13 mm (CM) compare well with values of other studies. For the Negev Desert, Israel, Kidron and Kronenfeld (2017) report NRWI values up to 0.1 mm for nights without fog, Jacobs et al. (2002) measured dew amounts ranging from 0.15 up to 0.3 mm and Heusinkveld et al. (2006) report "accumulated dew" in the range of 0.1 and 0.3 mm. For a coastal Steppe in Spain, Uclés et al. (2013) report average NRWI per night of 0.24 mm for bare soil and 0.16 mm for stones. Other published values of nightly dewfall in arid regions 0.08 mm (Goshute Valley, Nevada, Malek et al., 1999) and 0.01–0.1 mm (Atacama Desert, Chile, Kalthoff et al., 2006). Exceptionally higher values of NRWI ("fog was absent") were observed at Stellenbosch, South Africa, by Kaseke et al. (2012) for river sand with values of around 1 mm. For a comprehensive and up to date overview on maximum reported amounts of dew and fog the reader is referred to Table 1 in Kidron and Starinsky (2019).

For the separation of fog deposition and duration from dew and adsorption processes, an excess value of NRWI compared to the no-fog diurnal mean at a specific point in time is not sufficient, because the daily characteristics vary too much. We therefore took the difference between adjacent values of the mean diurnal curve, i.e. the mean deposition rate, as a reference and evaluated values against a threshold for the determination of the start of fog deposition. The time when the deposition rate on a certain night exceeds this threshold is considered as the beginning of a fog deposition event. The end of the deposition and thus the event is at the time of the maximum nightly deposition.

Fig. 10 shows an example of how the deposition duration is derived from the deposition rate and why a simple overshooting of the mean diurnal course is not applicable. Remarkably, the MLs at a specific location react almost simultaneously, which demonstrates the robustness of the ML construction and electronics. The start of fog deposition may occur suddenly (CM and GB), or continuously (VF). Thus, the definition of the threshold rate is crucial, especially in case of weak fog

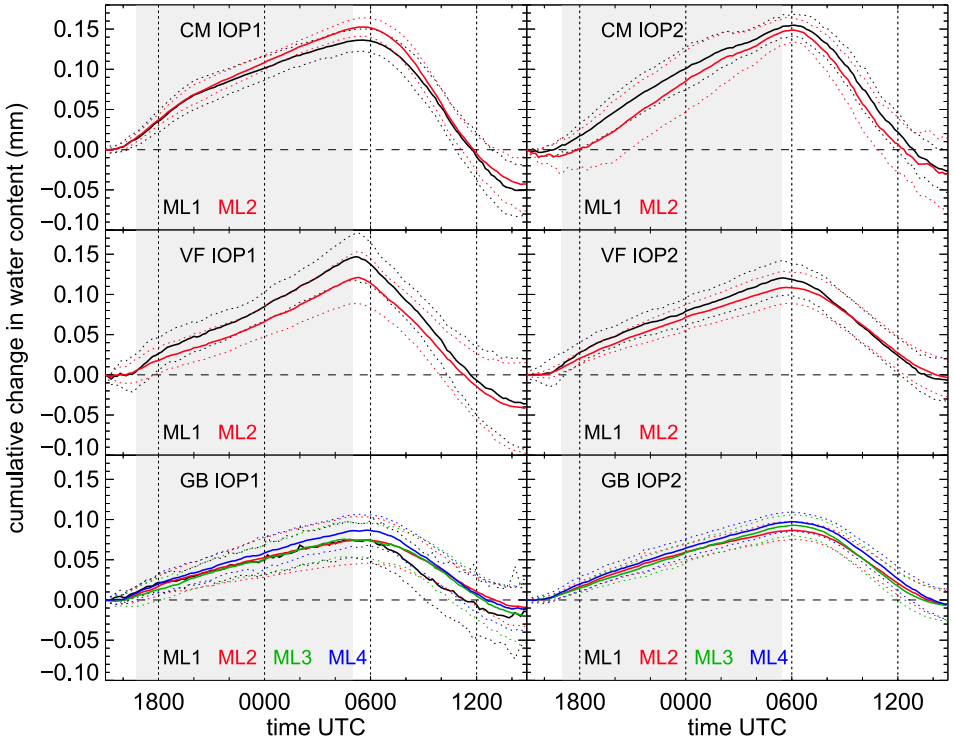

Fig. 9. Mean diurnal course of ML cumulative change of water content for days/nights without fog with standard deviations (dotted lines). Shaded areas refer to nightime (sunset to sunrise) for IOP 1 (left) and IOP 2 (right).

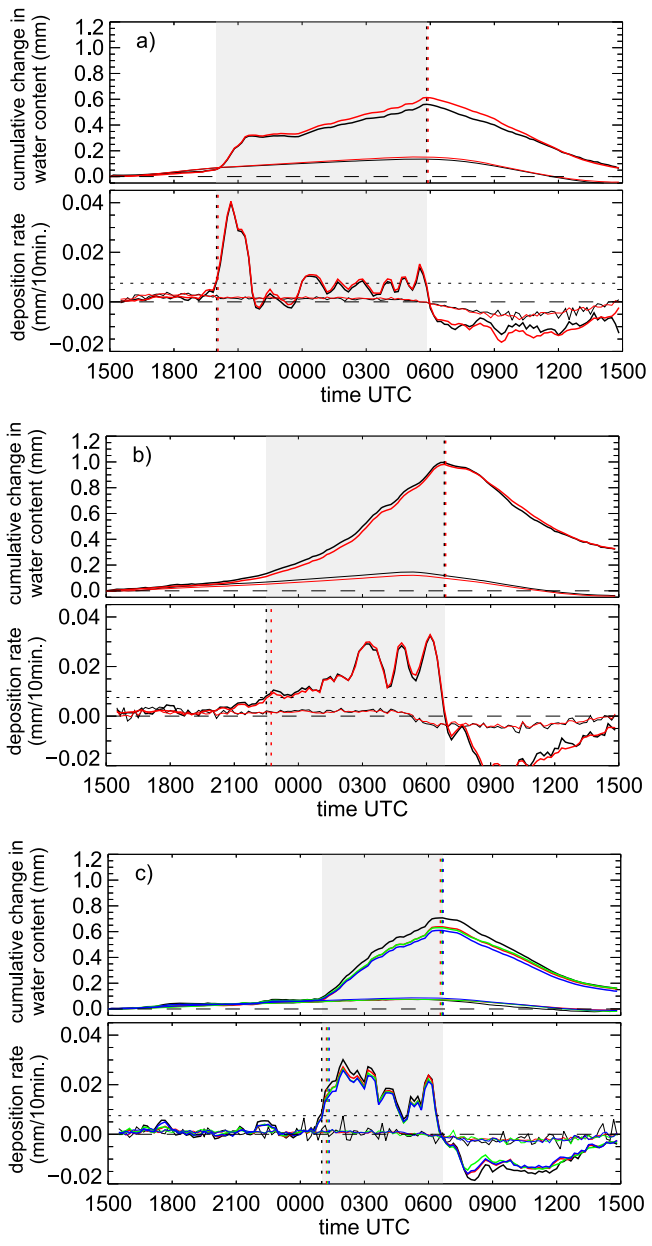

Fig. 10. a) upper panel: ML readings (solid thick) starting on 12 Sep 2017 at 1500 UTC and mean diurnal course during no-fog nights (solid thin) at CM. Vertical lines denote the time of the maximum. Lower panel: same as above but for change rate in water content. Horizontal dotted line denotes the threshold rate. Vertical lines define the start and are derived for each ML individually. Shaded area refers to fog deposition duration. b) and c) same as a) but for VF and GB.

events with little fog deposition. In our case, a value of 0.0075 mm increase over a 10-min interval was chosen for the start of fog deposition at all stations. For CM, further support for the selection of the threshold is provided. Here, the deposition started around 2000 UTC but stops after about 2 h, i.e. the threshold is no longer reached. After another 2 h the rate increases again and scatters around the threshold line until the end of the event at around 0600 UTC (maximum deposition). Fig. 10 illustrates a typical feature of the Namib fog in the investigation area. The advected marine stratus/fog front is first recorded closest to the coast at CM at around 2000 UTC. The front moves further inland, i.e. eastward, reaching VF at 2230 UTC, and, as wind comes from the north, finally reaches GB to the south of VF shortly after midnight. The stratus intercepts with the ground at all stations during this night, as is evident from the recorded fog deposition. Such a typical fog event is also shown for all FogNet stations in Fig. 7 in Spirig et al. (2019). For more details about the regional fog climatology and the general patterns of the Namib fog life cycle see e.g. Lancaster et al. (1984), Seely and Henschel (1998), Eckardt et al. (2013), Hachfeld and Jürgens (2000), Andersen et al. (2019) and Spirig et al. (2019) and references therein.

We calculated the duration of fog related events during the first phase of IOP1 (see Table 5) for different criteria using the thresholds given in Table 4.

Fig. 11 gives an overview on the duration calculations during the first phase of IOP1, where the most and strongest fog events occured. Theoretically fog occurs only if the air is saturated, however the threshold for relative humidity was set to 95% in order to account for the uncertainty of *RH* measurements by capacitive sensors in air close to saturation. The theoretical definitions of WVA and dew (see introduction) are used for calculating durations in Fig. 11, where blue colors denote periods for potential dew fall ($LST \leq T_{dew}$). WVA and dew formation cannot occur simultaneously by definition. Only a few periods fulfilled the conditions for dew fall at CM and GB, while the elevated site VF showed frequent periods where *LST* was below T_{dew}. These periods were related to clear-sky nights, which were more frequent in VF, and/or occasional break-up of the stratus during the night, which was also, but rarely, observed at GB. We therefore assume, that WVA and fog are the main vectors of NRWI on bare soil in the investigation area, as found in other studies (Uclés et al., 2013; Agam (Ninari) and Berliner, 2004b; Kaseke et al., 2012). Fog events in the investigation area are always connected to a stratus/low cloud intercepting with the ground. No fog deposition/precipitation was measured when the stratus did not intercept with the ground. Such situations were most common at CM, the site closest to the coast (e.g. 14 to 16 Sep). The occurrence and duration of stratus/low cloud can be accurately detected by the analysis of the nightly net radiation and short-wave downward radiation, if the stratus dissolves after sunrise (Spirig et al., 2019).

Visibility and leaf-wetness provide additional information about fog event durations. According to the international WMO definition, fog reduces visibility to values below 1000 m. Visibility was only measured at GB and is therefore not representative for the whole area of investigation. Furthermore the threshold of 1000 m is not low enough for the proper estimation of the duration of fog events as evident during the nights from 21 to 22 Sep and from 24 to 25 Sep, where visibility only fell below 1000 m for a short period at the beginning of the night while fog

Table 4
Variables and conditions for fog event duration calculation * GB only; ** Campbell Scientific, Ltd.

Variable/Symbol	Instrument/ manufacturer	Conditions and thresholds for start of event (night-time only)	end of event (if applicable)
relative humidity *RH*	CS215 temperature and *RH* probe, CS**	>95%	–
WVA from LST, T_{dew} and *RH*	IR120 radiometer, CS**	$LST > T_{dew}$, *RH* > 90%	–
Dew from LST and T_{dew}	IR120 radiometer, CS**	$LST \leq T_{dew}$	–
Net radiation Q*	Net radiometer Kipp&Zonen CNR4	$Q^* > -15$ W m^{-2} for $SW\downarrow < 0$ W m^{-2}	$0 < SW\downarrow < SW\downarrow_{clearsky}$
Short/Longwave down-/upwelling $SW\downarrow\uparrow$ $LW\downarrow\uparrow$			
Visibility *	Atm. Visibility monitor CS120A, CS**	<1000 m	–
Leaf wetness sensor	Model 237, CS**	<10 Ohm	–
Fog precipitation	Juvik fog collector	first tick	last tick
Fog deposition rate (mm/10min)	Microlysimeter, self-construction (see text)	>0.0075 mm/10 min.	max. deposition

Table 5
Selected parameters for each night (1500–1500 UTC) of the case study period from 24 Sep to 29 Sep 2017 * nights with no fog precipitation **with interruptions, see Fig. 13

night		Stratus (UTC)	NRWI (mm)	Fog prec. (ml)	$T_{dew} > LST$ (UTC)	$RH > 95\%$ (UTC)
24–25	CM	1840–0830	0.88	50		2200–0630
	VF	2040–0750	0.53	152	1920–0510	2020–0640
	GB	2210–0850	0.46	36		2220–0540
25–26	CM	0430–0730	0.27	12	2110–0600	0140–0640
	VF		*0.20*		1940–0610	2250–0520
	GB		*0.07*		0310–0510	
26–27	CM	0000–0840	0.22		2030–2400	2300–0010
	VF	0010–0450	0.40	290	1950–0600	2320–0520
	GB	0240–0610	*0.08*	56	0100–0220	0230–0650
27–28	CM	1940–0830	*0.14*			
	VF	2110–0540	0.39	164	1920–0520**	2050–0640
	GB	2220–0600	0.19	64		2210–0630
28–29	CM	0020–0730	0.25	18	2000–0020	2340–0610
	VF		*0.13*		2000–0600	0350–0430
	GB		*0.09*		0220–0510	

deposition/precipitation continued throughout the night. The leaf wetness sensors, placed at 0.1 m above the ground, serve as an indicator of the wetness of the soil surface. A value of 10 Ohm and lower represents to a wet surface (manufacturer term sheet/manual). Such situations were more common in CM compared to GB. However, it seems that the leaf wetness sensor, though placed as close to the surface as possible, is not strictly representative of soil surface wetting. As mentioned above, situations for potential dew formation were frequent at VF. During these nights (e.g. 13, 15, 20, 25 and 29 Sep), the leaf wetness sensor was wet almost during the whole night, yet no significant additional dew deposition was measured by the MLs. This implies that dew rarely forms on bare desert soils, confirming the findings in Agam and Berliner (2002, 2006).

3.2. Gain (NRWI) and loss (evaporation) of soil water

The offset corrected curves of MLs (Fig. 2) reflect the general features of fog spatial distribution and seasonality in the Central Namib with the highest NRWI at the coast (CM) and at the elevated VF site during the high fog season in Sep/Oct. Generally, lower NRWI values were recorded at the inland sites in Feb/Mar due to fewer occurring fog events.

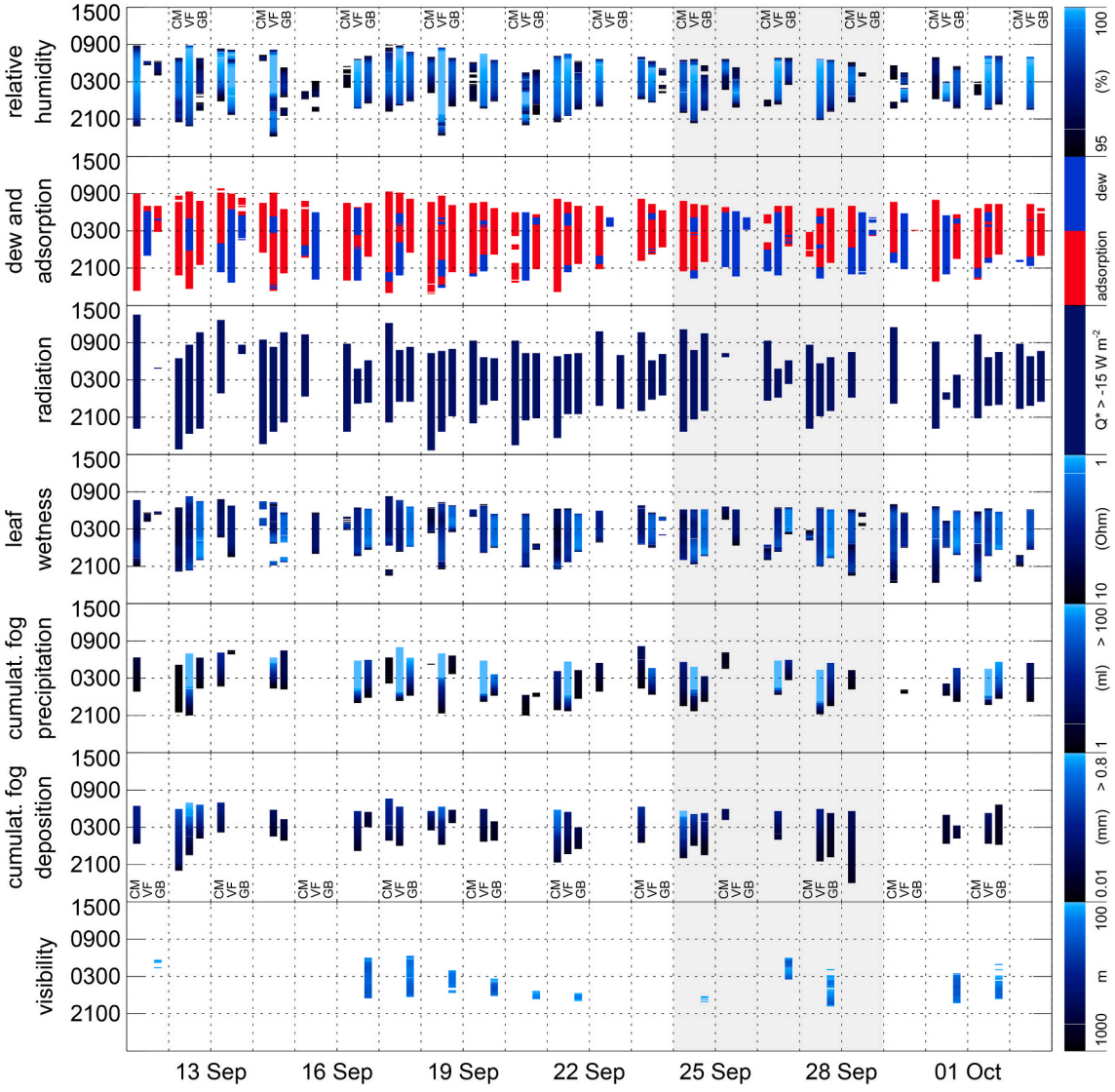

Fig. 11. Durations of stratus/low cloud and fog events for the first phase of IOP1 in CM, VF and GB (bars for each day from left to right) for selected measures according to thresholds listed in Table 4. Visibility (lowest panel) was only measured at GB. Shaded period refers to case study period analyzed in section 4. Time refers to UTC.

After the nightly maximum of ML water content is reached, usually shortly before sunrise, evaporation starts because of solar input. A trend analysis of ML raw data allows the estimation of gain/loss of soil water during a certain period, but, due to the drawbacks of relative calibration, offsets and sudden weight changes (see section 1), the inspection of daily cycles of the complete time series yields more robust results. Following the daily decomposition of the ML data, the last value of a daily cycle refers to either gain (positive, NRWI) or loss (negative, evaporation) of soil water. Since the investigation area is hyper-arid and the last significant rainfall (>0.5 mm/day) was registered in mid-August 2017, water availability was limited, and the soils were consequently very dry. In general, all NRWI evaporated by the end of a daily cycle, but after heavy fog events, it took another day or two, as evident by the imbalance between gain and loss for single days (Fig. 12a).

The first phase of IOP1 (11 Sep to 2 Oct) experienced the most fog events with high deposition at all stations (Fig. 12a). After heavy fog events (12, 18 (VF), 21 and 24 Sep) with high NRWI, evaporation is also high but does not fully compensate for the gain of soil water from the preceding night. Consequently, evaporation exceeds NRWI slightly for another two or three days, either until the next fog event occurs or until all available water evaporated and the formerly described no-fog diurnal cycle is re-established. This extended impact of strong events is

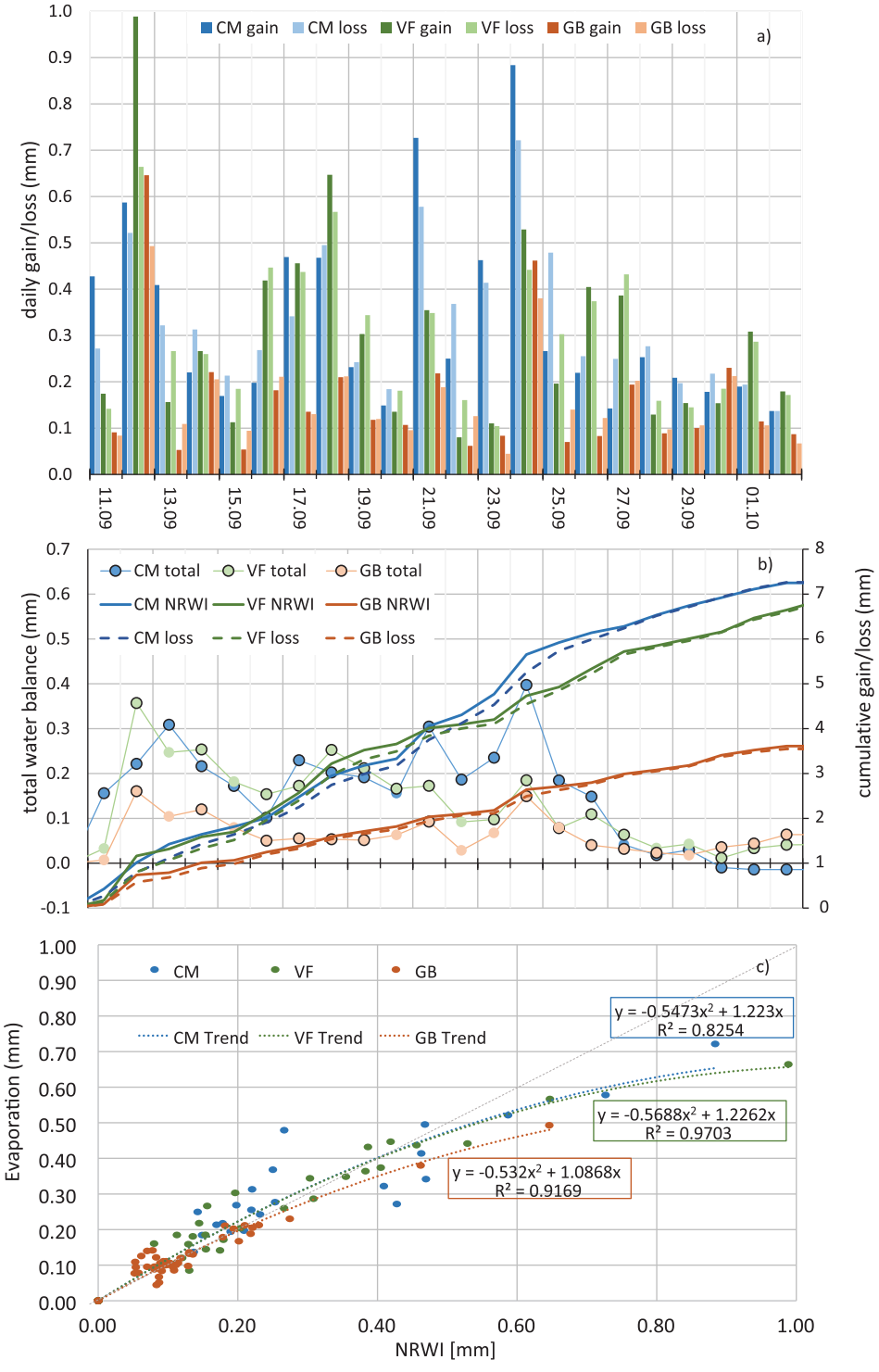

Fig. 12. a) Daily gain and loss of soil water during the first phase of IOP1 at CM (blue), VF (green) and GB (red). Dark colored bars denote daily NRWI (gain), bars in light colors refer to evaporation (loss) at the end of each 24 h daily cycle (1500-1500 UTC). b) as a) but for cumulative sums of NRWI (gain) and evaporation (loss), (right scale, thick solid lines and dashed lines, respectively) and cumulative water balance (left scale, lines with bullets). Black circled bullets mark days with recorded fog precipitation, x-axis same as a). c) NRWI plotted against evaporation with a trendline. (For interpretation of the references to color in this figure legend, the reader is referred to the Web version of this article.)

supported by the relation between daily NRWI and evaporation (Fig. 12c) with high coefficients of determination R^2 of 0.83, 0.97 and 0.92 for CM, VF and GB, respectively. The fitted curves suggest a 1:1 relation until an NRWI of about 0.4 mm, based on no-fog days and moderate fog events. Above this value, evaporation during the following day is no longer high enough to compensate for the NRWI due to the heavy fog of the preceding night. A small gain results at VF and GB sites for the selected period due to the numerous fog events (Fig. 12b), but at the end of each IOP, the ML balance is close to zero as shown in Fig. 2. The highest daily depositions were observed at CM and VF with nearly 1 mm, each on a different day.

Despite several common features (advection of stratus/low cloud from the coast to inland and interception with the ground) which allow the derivation of a robust fog climatology for the area of investigation, we will show in the following section details of selected events exhibiting essential differences with respect to the relation of fog deposition and fog precipitation as the principal measures of the intensity and strength of a fog event.

4. Case study period

The 5-day period from 24 Sep to 29 Sep 2017 is chosen because it demonstrates the variability of fog events in the region of investigation and at the three FogNet stations equipped with MLs in detail. The relevant time series of fog deposition, fog precipitation, net radiation, relative humidity, air temperature, surface temperature, dew point temperature, wind velocity and wind direction are displayed in Fig. 13.

Starting with the night from 24 to 25 Sep the region experienced a strong fog event with high fog deposition and fog precipitation registered at all three stations. The stratus was present close to the coast (CM) from the beginning of the night at 1840 and reached inland stations VF and GB at 2040 and 2210 UTC, respectively. While the start of fog precipitation and deposition at CM was delayed by about 2 h, they started simultaneously with stratus arrival at VF and GB, indicating that the arriving stratus intercepted with the ground. The highest amount of fog precipitation was measured at the elevated site VF (515 m a.s.l.) with 152 ml while highest fog deposition occurred at CM with 0.88 mm. Though weak conditions for dew formation were given during the second half of night at VF with $T_{dew} \cong LST$, we attribute the NRWI to fog deposition because there was no further radiative cooling of the surface (as observed in the following night) and fog deposition was in the same range as in GB.

Two similar nights (25–26 and 28–29 Sep) exhibited clear skies as indicated by the strong negative net radiation Q* at all stations. Shortly before sunrise small amounts of fog deposition (0.27 and 0.25 mm) and fog precipitation (36 and 18 ml) were recorded at CM, but the stratus did not proceed further inland. Conditions for dew formation were given during the whole night at VF and for a short period shortly before sunrise at GB. Both nights showed strong radiative cooling at VF resulting in differences between *LST* and T_{dew} of up to 5 K. The ML reading in the night from 25–26 Sep with 0.2 mm exceeded the mean threshold of 0.11 mm derived for no-fog nights at VF (see section 3.1). The difference of 0.09 mm could be interpreted as additional NRWI according to dew, i.e. water vapour condensed on the bare soil surface, especially in the early

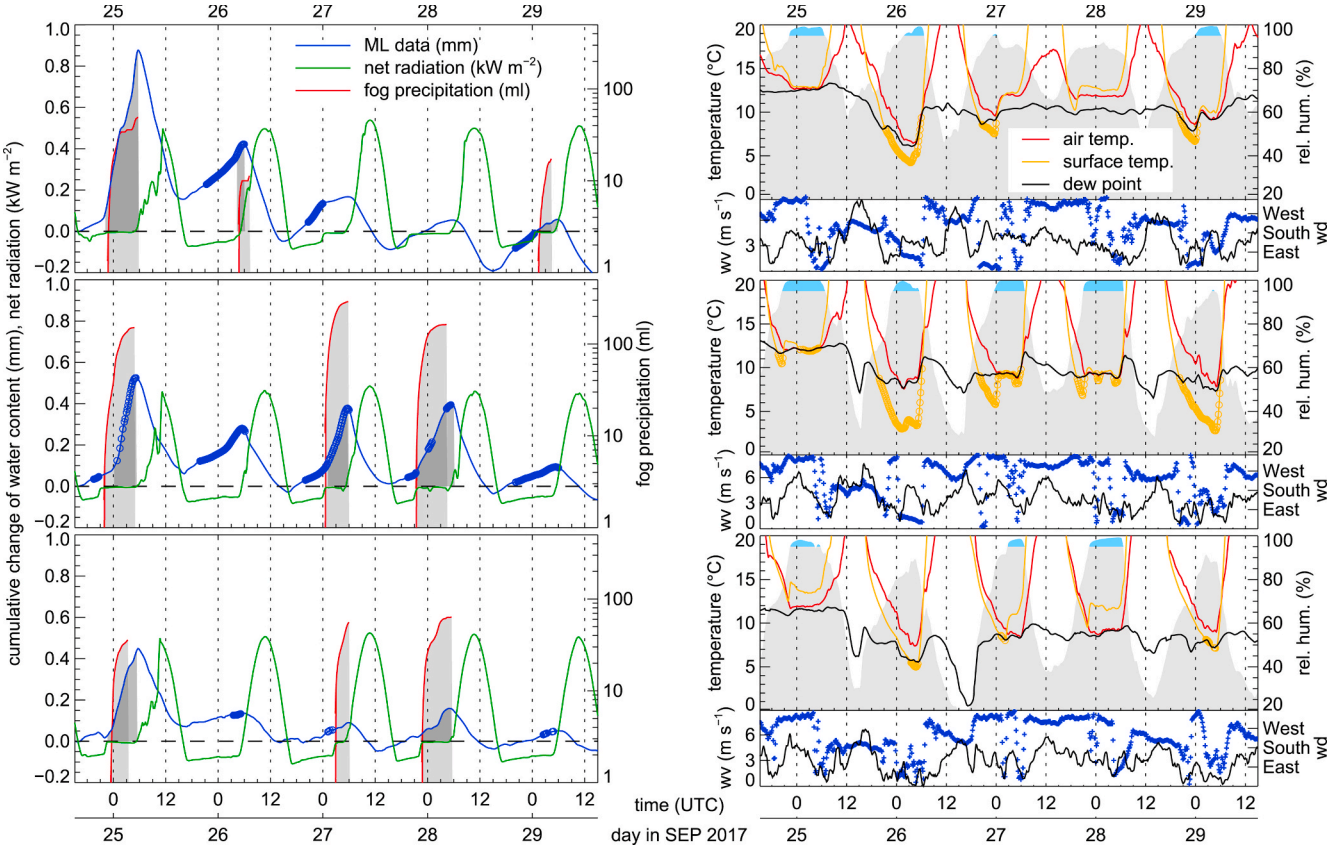

Fig. 13. Fog events during the period from 24 SEP 1500 UTC to 29 SEP 2017 1500 UTC at CM, VF and GB (from top to bottom). Left panel: Cumulative change of water content (blue solid, circles refer to periods where LST ≤ Tdew), net radiation Q* (green solid) and fog precipitation (red solid, log scale right y-axis). Shaded areas refer to the respective duration of events, dark grey areas indicate overlapping of fog deposition and fog precipitation durations. Right panel, upper part: Air temperature Tair (red solid), Land Surface Temperature LST (orange solid, circles refer to periods where LST ≤ Tdew) and dew point temperature Tdew (black solid). Shaded areas refer to relative humidity RH (scales with right y-axis), light blue areas indicate periods with RH > 95%. Right panel, lower part: wind velocity (black solid) and wind direction (blue symbols, scales with right y-axis). (For interpretation of the references to color in this figure legend, the reader is referred to the Web version of this article.)

morning, when the deposition rate was increasing. During the night from 28–29 Sep with similar radiative cooling conditions, but lower relative humidity, this difference was only 0.02 mm, which is well in the range of the variation of the mean diurnal course (Fig. 9). Kidron and Kronenfeld (2017) estimated that "more than 7 h of optimal conditions" (with respect to *RH*, *LST* and T_{dew}) are required for dew formation on bare soil. These conditions were not met long enough during this night but during the night from 25–26 Sep. This exemplifies the difficulties to assess the contribution of dew to NRWI, and, in detail, to provide evidence of dew formation on bare soil in hyper-arid environments, as addressed earlier in this study.

Fog precipitation was measured in the consecutive nights from 26–27 Sep and 27–28 Sep inland (VF and GB), but not at the coast (CM). The total NRWI of 0.22 mm at CM from 26–27 Sep probably contains a small contribution from dew formation due to radiative cooling during the first half of the night ($LST < T_{dew}$ and increased deposition rate). The stratus arrived at midnight but obviously did not intercept with the ground in CM, similar as in the following night when stratus was present during the whole night but neither fog deposition nor fog precipitation were recorded at CM. In contrast, VF experienced high amounts of fog precipitation (290 ml and 164 ml) and NRWI due to fog (0.40 and 0.39 mm) immediately upon stratus arrival (0010 and 2110, respectively). The stratus arrived at GB about 1–2 h later (0240 and 2220). Fog precipitation was also high at GB (56 and 64 mm), but no NRWI due to fog was measured in the night from 26–27 Sep. These two nights show exemplarily the discrepancies in the relation between fog precipitation and fog deposition. High amounts of fog precipitation do not necessarily infer that fog deposition occurs and though similar amounts of NRWI were measured on both nights at VF, the amounts of fog precipitation differed substantially.

The detailed analysis of the case study period reveals the complex interaction of the drivers defining amount and duration of a fog event, i.e. fog deposition, fog precipitation, relative humidity, stratus occurrence and interception with the ground and other parameters as shown in Fig. 11. Though there were some common essential preconditions for a fog event in the region of investigation like air close to saturation and stratus interception with the ground, the quantification of NRWI and fog precipitation showed substantial differences during the individual events and a clear relationship was not evident in the frame of this research. A deeper analysis assessing the relationship between these two significant hydrological parameters is certainly needed but out of the scope of this study.

5. Conclusions

We showed that the presented self-constructed microlysimeters are a simple and robust tool to detect even smallest amounts of NRWI (non-rainfall water input), i.e. adsorption water, dew and fog deposition in arid environments. NRWI occurs essentially between sunset and sunrise and usually evaporates completely during the following day, except after heavy fog events. In these cases, the water balance recovers during the following 1–2 days, provided that no further fog events occur during this period. A possible explanation is given by Daamen and Simmonds (1996): soil surface resistance is increasing with decreasing water content in the uppermost soil layer during the day and limits the total daily potential evaporation.

The diurnal variation of microlysimeter readings during no-fog days/nights turned out to be very consistent. This allows to determine the duration of fog deposition during fog events using a site specific threshold of total deposition and of deposition rate (0.075 mm/10 min in our case). NRWI due to fog starts when the deposition rate exceeds the threshold and ends with the maximum of microlysimeter reading. During no-fog days/nights, NRWI by adsorption usually starts in the late afternoon and ends with sunrise.

Stratus/low cloud occurrence is required for a fog event and can be easily detected in the radiation signal. Fog deposition/precipitation is recorded when a stratus/low cloud intercepts with the ground, which is predominantly the case at inland stations due to the rising terrain of the escarpment.

Fog event duration is determined by the ongoing occurrence of fog precipitation and/or fog deposition together with low visibility, low cloud base and high leaf wetness. However, no correlation was found between fog precipitation (measured by Juvik-type fog samplers) and fog deposition. Nights with fog precipitation but without fog deposition were observed and vice versa. To date we could not find any systematic reason for that but analysis of droplet size distributions, measured by a cloud droplet probe, may provide further insight. Further research is needed to answer how much of the water sampled by fog collectors actually reaches the ground as a component of NRWI, how the two sampling methods differ with respect to the relevant processes in fog and how much it contributes to the water budget of a specific site in the short and the long term.

CRediT authorship contribution statement

Christian Feigenwinter: Conceptualization, Methodology, Formal analysis, Writing - original draft, Visualization. **Joel Franceschi:** Investigation, Data curation. **Jarl Are Larsen:** Resources, Investigation, Data curation, Software. **Robert Spirig:** Investigation, Writing - review & editing. **Roland Vogt:** Project administration, Investigation, Writing - review & editing.

Declaration of competing interest

The authors declare that they have no known competing financial interests or personal relationships that could have appeared to influence the work reported in this paper.

Acknowledgements

Funding for this study was provided by the Swiss National Science Foundation (SNSF) for CF, RS and JAL (Grant 163291, NaFoLiCA). Edward Martins from Telecom Namibia provided easy access to the area of Coastal Met. We thank the staff of the Gobabeb Research and Training Center for the support during the IOPs. H.R. Rüegg from UNIBAS is highly acknowledged for microlysimeter engineering and drawings.

References

Agam (Ninari), N., Berliner, P.R., 2004b. Diurnal water content changes in the bare soil of a coastal desert. J. Hydrometeorol. 5, 922–933.
Agam, N., 2014. Comment on "Microlysimeter station for long term non-rainfall water input and evaporation studies" by Uclés et al. Agric. For. Meteorol. 194, 255–256.
Agam, N., Berliner, P.R., 2006. Dew formation and water vapour adsorption in semi-arid environments—a review. J. Arid Environ. 65, 572–590.
Agam, N., Berliner, P.R., 2004. Soil water evaporation during the dry season in an arid zone. J. Geophys. Res. 109, D16103. https://doi.org/10.1029/2004JD004802.
Alduchov, O.A., Eskridge, R.E., 1996. Improved Magnus form approximation of saturation vapor pressure. J. Appl. Meteorol. Climatol. 35, 601–609.
Andersen, H., Cermak, J., Solodovnik, I., Lelli, L., Vogt, R., 2019. Spatiotemporal dynamics of fog and low clouds in the Namib unveiled with ground- and space-based observations. Atmos. Chem. Phys. 19 (7), 4383–4392. https://doi.org/10.5194/acp-19-4383-2019.
Aubinet, M., Vesala, T., Papale, D., 2012. Eddy Covariance: A Practical Guide to Measurement and Data Analysis. *Springer Atmospheric Sciences*, Springel Netherlands. ISBN 9400723512, 9789400723511.
Beiderwieden, E., Wolff, V., Hsia, Y.-J., Klemm, O., 2008. It goes both ways: measurements of simultaneous evapotranspiration and fog droplet deposition at a montane cloud forest. Hydrol. Process. 22, 4181–4189.
Beysens, D., Muselli, M., Nikolayev, V., Narhe, R., Milimouk, I., 2005. Measurement and modelling of dew in island, coastal and alpine areas. Atmos. Res. 73, 1–22. https://doi.org/10.1016/j.atmosres.2004.05.003.
Daamen, C.C., Simmonds, L.P., 1996. Measurement of evaporation from bare soil and its estimation using surface resistance. Water Resour. Res. 32, 1393–1402.
Demoz, B.B., Collett Jr., J.L., Daube Jr., B.C., 1996. On the caltech active strand cloudwater collectors. Atmos. Res. 41, 47–62.
Duvdevani, S., 1947. An optical method of dew estimation. Q. J. Roy. Meteorol. Soc. 73, 282–296. https://doi.org/10.1002/qj.49707331705.

Eckardt, F., Soderberg, K., Coop, L., Muller, A., Vickery, K., Grandin, R., Jack, C., Kapalanga, T., Henschel, J., 2013. The nature of moisture at Gobabeb, in the central Namib Desert. J. Arid Environ. 93, 7–19. https://doi.org/10.1016/j.jaridenv.2012.01.011.

Eugster, W., Burkard, R., Holwerda, F., Scatena, F.N., Bruijnzeel, L.A., 2006. Characteristics of fog and fogwater fluxes in a Puerto Rican elfin cloud forest. Agric. For. Meteorol. 139, 288–306.

Feigenwinter, C., Bernhofer, C., Eichelmann, U., Heinesch, B., Hertel, M., Janous, D., Kolle, O., Lagergren, F., Lindroth, A., Minerbi, S., Moderow, U., Mölder, M., Montagnani, M., Queck, R., Rebmann, C., Vestin, P., Yernaux, M., Zeri, M., Ziegler, W., Aubinet, M., 2008. Comparison of horizontal and vertical advective CO_2 fluxes at three forest sites. Agric. For. Meteorol. 148, 12–24. https://doi.org/10.1016/j.agrformet.2007.08.013.

Fernandez, D.M., Torregrosa, A., Weiss-Penzias, P.S., Zhang, B.J., Sorensen, D., Cohen, R. E., McKinley, G.H., Kleingartner, J., Oliphant, A., Bowman, M., 2018. Fog water collection effectiveness: mesh intercomparisons. Aerosol and Air Quality Research 18, 270–283. https://doi.org/10.4209/aaqr.2017.01.0040.

Florentin, A., Agam, N., 2017. Estimating non-rainfall-water-inputs-derived latent heat flux with turbulence-based methods. Agric. For. Meteorol. 247, 533–540. https://doi.org/10.1016/j.agrformet.2017.08.035, 2017.

Frumau, K.F.A., Burkard, R., Schmid, S., Bruijnzeel, L.A., Tobón, C., Calvo-Alvarado, J. C., 2011. A comparison of the performance of three types of passive fog gauges under conditions of wind-driven fog and precipitation. Hydrol. Process. 25, 374–383.

Gerber, H., 1991. Direct measurement of suspended particulate volume concentration and far-infrared extinction coefficient with a laser-diffraction instrument. Appl. Optic. 30, 4824–4831.

Goodman, J., 1985. The collection of fog drip. Water Resour. Res. 21 (3), 392–394.

Graf, A., Kuttler, W., Werner, J., 2004. Dewfall measurements on lanzarote, canary islands. Meteorol. Z. 13 (5), 405–412.

Grunow, J., 1952. Nebelniederschlag. *Ber. Deutsch. Wetterd. U.S. Zone 7*. Bad Kissinger 42, 30–34.

Hachfeld, B., Jürgens, N., 2000. Climate patterns and their impact on the vegetation in a fog driven desert: the Central Namib Desert in Namibia. Phytocoenologia 30, 567–589. https://doi.org/10.1127/phyto/30/2000/567.

Henschel, J.R., Lancaster, N., 2013. Gobabeb – 50 years of Namib Desert research. J. Arid Environ. 93, 1–6. https://doi.org/10.1016/j.jaridenv.2012.09.015.

Heusinkveld, B.G., Berkowicz, S.M., Jacobs, A.F.G., Holtslag, A.A.M., Hillen, W.C.M., 2006. An automated microlysimeter to study dew formation and evaporation in arid and semiarid regions. J. Hydrometeorol. 7 (4), 825–832. https://doi.org/10.1175/JHM523.1.

Jacobs, A.F.G., Heusinkveld, B.G., Berkowicz, S.M., 1999. Dew deposition and drying in a desert system: a simple simulation model. J. Arid Environ. 42 (3), 211–222.

Jacobs, A.F.G., Heusinkveld, B.G., Berkowicz, S.M., 2002. A simple model for potential dewfall in an arid region. Atmos. Res. 64, 285–295.

Juvik, J.O., Nullet, D., 1995. Comments on "A proposed Standard Fog Collector for use in high-elevation regions". J. Appl. Meteorol. 34, 2018–2110.

Kalthoff, N., Fiebig-Wittmaack, M., Meißner, C., Kohler, M., Uriarte, M., Bischoff-Gauß, I., Gonzales, E., 2006. The energy balance, evapo-transpiration and nocturnal dew deposition of an arid valley in the Andes. J. Arid Environ. 65, 420–443. https://doi.org/10.1016/j.jaridenv.2005.08.013.

Kaseke, K.F., Wang, L., Seely, M.K., 2017. Nonrainfall water origins and formation mechanisms. Sci. Adv. 3 (3), 1–8. https://doi.org/10.1126/sciadv.1603131.

Kaseke, K.F., Mills, A.J., Brown, R., Esler, K.J., Henschel, J.R., Seely, M.K., 2012. A method for direct assessment of the "Non Rainfall" atmospheric water cycle: input and evaporation from the soil. Pure Appl. Geophys. 169, 847–857. https://doi.org/10.1007/s00024-011-0328-9.

Kidron, G.J., Kronenfeld, R., 2017. Assessing the effect of micro-lysimeters on NRWI: do micro-lysimeters adequately represent the water input of natural soil? J. Hydrol. 548, 382–390. https://doi.org/10.1016/j.jhydrol.2017.03.005.

Kidron, G.J., Starinsky, A., 2019. Measurements and ecological implications of non-rainfall water in desert ecosystems – a review. Ecohydrology, e2121. https://doi.org/10.1002/eco.2121.

Kidron, G.J., 2000. Analysis of dew precipitation in three habitats within a small arid drainage basin, Negev Highlands, Israel. Atmos. Res. 55, 257–270. https://doi.org/10.1016/S0169-8095(00)00063-6.

Klemm, O., Wrzesinsky, T., Scheer, C., 2005. Fog water flux at a canopy top: direct measurement versus one-dimensional model. Atmos. Environ. 39, 5375–5386.

Lancaster, J., Lancaster, N., Seely, M.K., 1984. Climate of the central Namib Desert. Madoqua 14 (1), 5–61.

Lee, X., 1998. On micrometeorological observations of surface-air exchange over tall vegetation. Agric. For. Meteorol. 91, 39–49.

Malek, E., McCurdy, G., Giles, G., 1999. Dew contribution to the to the annual water balances in semi-arid desert valleys. J. Arid Environ. 42, 71–80.

Mendelsohn, J., Jarvis, A., Roberts, C., Robertson, T., 2002. Atlas of Namibia: A Portrait of the Land and its People. David Philip Publishers, Cape Town, South Africa.

Mitchell, D., Henschel, J.R., Hetem, R.S., Wassenaar, T.D., Strauss, W.M., Hanrahan, S. A., Seely, M.K., 2020. Fog and fauna of the Namib Desert: past and future. Ecosphere 11 (1), e02996. https://doi.org/10.1002/ecs2.2996.

Ninari, N., Berliner, P.R., 2002. The role of dew in the water and heat balance of bare loess soil in the Negev Desert: quantifying the actual dew deposition on the soil surface. Atmos. Res. 64, 323–334.

Price, J.D., Clark, R., 2014. On the measurement of dewfall and fog-droplet deposition. Bound.-Layer Meteorol. 152, 367–393. https://doi.org/10.1007/s10546-014-9930-6.

Qin, Z., Berliner, P., Karnieli, A., 2005. Ground temperature measurement and emissivity determination to understand the thermal anomaly and its significance on the development of an arid environmental ecosystem in the sand dunes across the Israel–Egypt border. J. Arid Environ. 60, 27–52. https://doi.org/10.1016/j.jaridenv.2004.03.017.

Regalado, C.M., Ritter, R., 2016. The design of an optimal fog water collector: a theoretical analysis. Atmos. Res. 178–179, 45–54.

Regalado, C.M., Ritter, R., 2017. The performance of three fog gauges under field conditions and its relationship with meteorological variables in an exposed site in Tenerife (Canary Islands). Agric. For. Meteorol. 233, 80–91.

Rivera, J., 2011. Aerodynamic collection efficiency of fog water collectors. Atmos. Res. 102, 335–342.

Schemenhauer, R.S., Cereceda, P., 1994. A proposed Standard Fog Collector for use in high-elevation regions. J. Appl. Meteorol. 33, 1313–1322.

Seely, M., Henschel, J.R., 1998. The climatology of Namib fog. In: Proceedings of the First International Conference on Fog and Fog Collection, pp. 353–356, 19–24 July 1998, Vancouver.

Spiegel, J.K., Zieger, P., Bukowiecki, N., Hammer, E., Weingartner, E., Eugster, W., 2012. Evaluating the capabilities and uncertainties of droplet measurements for the fog droplet spectrometer (FM-100). Atmos. Meas. Tech 5, 2237–2260. https://doi.org/10.5194/amt-5-2237-2012.

Spirig, R., Vogt, R., Larsen, J.A., Feigenwinter, C., Wicki, A., Franceschi, J., Parlow, E., Adler, B., Kalthoff, N., Cermak, J., Andersen, H., Fuchs, J., Bott, A., Hacker, M., Wagner, N., Maggs-Kölling, G., Wassenaar, T., Seely, M.K., 2019. Probing the fog life cycle in the central Namib Desert. Bull. Am. Meteorol. Soc. 100 (12), 2491–2507. https://doi.org/10.1175/BAMS-D-18-0142.1.

Uclés, O., Villagarcía, L., Canton, Y., Domingo, F., 2013. Microlysimeter station for long term non-rainfall water input and evaporation studies. Agric. For. Meteorol. 182–183, 13–20.

Uclés, O., Villagarcía, L., Moro, M.J., Canton, Y., Domingo, F., 2014. Role of dewfall in the water balance of a semiarid coastal steppe ecosystem. Hydrol. Process. 28, 2271–2280. https://doi.org/10.1002/hyp.9780.

Wang, L., Kaseke, F., Seely, M., 2017. Effects of non-rainfall water inputs on ecosystem functions. WIREs Water 4, e1179. https://doi.org/10.1002/wat2.1179.

Wrzesinsky, T., Scheer, C., Klemm, O., 2004. Fog deposition and its role in biogeochemical cycles of nutrients and pollutants. In: Matzner, E. (Ed.), Biogeochmistry of Forested Catchments in a Changing Environment, a German Case Study. *Ecological Studies*, 172. Springer, Heidelberg, pp. 191–202.

Zheng, J., Peng, C., Li, H., Li, S., Huang, S., Hu, Y., Zhang, J., Li, D., 2018. The role of non-rainfall water on physiological activation in desert biological soil crusts. J. Hydrol. 556, 790–799. https://doi.org/10.1016/j.jhydrol.2017.12.003.